

In situ deposition of Pd nanoparticles on carbon paper and their electroactivity for ethanol oxidation

Yuanyuan Zhang¹ · Qingfeng Yi¹ · Tao Zou¹ · Xiulin Zhou¹ · Huidong Nie¹

Received: 11 January 2017 / Revised: 11 April 2017 / Accepted: 14 April 2017 / Published online: 25 April 2017
© Springer-Verlag Berlin Heidelberg 2017

Abstract In this work, Pd and PdNi nanostructured particles have been deposited on the carbon paper (CP) by a novel and simple method of in situ deposition. The prepared catalysts were named as Pd-situ/CP, PdNi-situ/CP. The as-formed Pd and Pd-Ni nanoparticles are well dispersed with the sizes of 15~24 nm for Pd-situ/CP, 8~11 nm for Pd₉Ni₁-situ/CP, and 8~14 nm for Pd₈Ni₂-situ/CP. Their electroactivity for ethanol oxidation in 1 mol L⁻¹ NaOH solution was investigated with cyclic voltammetry, chronoamperometry, and electrochemical impedance spectroscopy. The samples fabricated by this in situ deposition method (Pd-situ/CP, Pd₉Ni₁-situ/CP, and Pd₈Ni₂-situ/CP) exhibit both higher electroactivity and higher electrocatalytic stability for ethanol oxidation than the Pd/CP obtained by the conventional NaBH₄ reduction method. This new method of preparation of catalyst nanoparticles is simple and hardly leads to the loss of catalyst particles due to the omitted filtration step of catalyst particles.

Keywords Ethanol oxidation · Pd electrocatalyst · Carbon paper · In situ deposition

Introduction

Membrane electrode assembly (MEA) is the key component of direct fuel/or liquid fuel cells. A MEA is generally fabricated by coating the anode catalyst and cathode catalyst particles on the respective side of a proton exchange membrane and

then pressing a gas diffusion layer (normally, a porous carbon paper) on both the anode catalyst and cathode catalyst. In other words, carbon paper (CP), anode catalyst, membrane, cathode catalyst, and CP are sequentially integrated to form a coherent whole. MEA has been extensively applied to various fuel cells like direct H₂/O₂ fuel cell [1–5], direct HCOOH/O₂ fuel cell [6–10], and direct alcohol/O₂ fuel cell [11–15]. As for the direct liquid fuel cells, ORR takes place in a three-phase region: electrolyte/oxygen gas/catalyst. CP is not only used as the catalyst support, but also used as the channel of transferring gas and discharging water formed from ORR.

Regarding the construction steps of the MEA, catalysts need to be prepared separately, which includes several steps of operation [16–21]. Firstly, a support like carbon powder and carbon nanotubes and metallic salts such as the metal precursors were mixed in a solvent under stirring and a reduction agent solution like NaBH₄ dissolved in water or ethylene glycol was subsequently added dropwise under stirring to form the black suspension. Followed by filtration and washing, the obtained catalyst particles were dried in a vacuum and put aside. Then, the catalyst particles, a solvent (water or alcohol), and a binder (generally Nafion solution) were mixed under sonication to form a uniform suspension (called ink). This ink was finally coated on a proton exchange membrane or on CP to fabricate a MEA. It is quite clear that there are lots of deficiencies for the conventional preparation of the catalyst particles: (1) the preparation process is cumbersome, (2) the amount of the catalyst particles may be reduced a little due to the filtration and washing steps, and (3) some catalyst particles may be aggregated together during their filtration and storage. It is therefore significant to develop a new preparation method of catalyst nanoparticles. Rego and coworkers reported the preparation of Pd nanoparticles directly deposited on porous CP by electroless deposition [22]. CP was firstly subjected to the necessary treatment of sensibilization/activation step by

✉ Qingfeng Yi
yqfyy2001@hnust.edu.cn

¹ School of Chemistry and Chemical Engineering, Hunan University of Science and Technology, Xiangtan 411201, China

successively immersing the CP in SnCl_2 and PdCl_2 solutions. The as-treated CP was then immersed in a Pd electroless solution ($27 \text{ mmol L}^{-1} \text{ N}_2\text{H}_4$, $28 \text{ mmol L}^{-1} \text{ Pd}^{2+}$, $0.1 \text{ mol L}^{-1} \text{ EDTA}$, $600 \text{ mL NH}_4\text{OH}$) at room temperature to let the formed Pd nanoparticles be deposited on the CP. In this electroless deposition, the formation of Pd nanoparticles and their deposition on CP were carried out separately. In other words, Pd nanoparticles were firstly produced in places outside CP, and subsequently, some particles were immobilized on CP. This would of course lead to the loss of the Pd nanoparticles. In addition, larger-size Pd particles were formed with this electroless deposition.

It is generally known that Pd-based catalysts present excellent electrocatalytic activity for ethanol oxidation in alkaline media [23, 24]. Among them, Pd-Ni [10, 17, 20, 21], Pd-Sn [21, 25–27], Pd-Pt [28–30], and Pd-metal oxide [31–34] have been paid considerable attention. In addition, binary Pd-Ni catalysts present efficient electroactivity for ethanol oxidation. Recently, we synthesized Pd_xNi_y /multiwalled carbon nanotube (CNT) catalysts by in situ deposition of Pd nanoparticles on Ni particles [17]. Results revealed that $\text{Pd}_{3.7}\text{Ni}_1/\text{MWCNT}$ catalyst exhibits a peak current density of $130.9 \text{ mA cm}^{-2} \mu\text{g}^{-1}$ (Pd), showing the excellent electrocatalytic activity of the Pd-Ni catalyst for ethanol oxidation.

In this work, a novel preparation method of Pd/PdNi nanoparticles by in situ deposition onto a porous CP using metallic salt as the precursor has been proposed and investigated. The metal precursor was firstly immobilized onto the porous CP by Nafion solution, and after drying, the metal salt-loaded CP was immersed in aqueous NaBH_4 solution, leading to the formation of metal nanoparticles which were in situ deposited on CP. This new method of preparation of catalyst nanoparticles is very simple and can be easily used to synthesize the CP-loaded metal nanoparticles uniformly dispersed on CP with small sizes. The as-fabricated CP-loaded Pd (PdNi) nanocatalysts were characterized by TEM and X-ray diffractogram (XRD) techniques, and their electroactivity for ethanol oxidation was studied in alkaline media.

Experimental

All chemicals used in this work, including sodium hydroxide, palladium chloride, nickel(II) chloride, sodium borohydride, and ethanol, were of analytical grade and used as received without further purification. Pure water ($18.2 \text{ M}\Omega \text{ cm}$) was obtained by double distillation of deionized water. CP (thickness = 0.3 mm , porosity = 75%) and Nafion solution (5% , Dupont) were purchased from Sinopharm Group Chemical Reagent Co. Ltd. Synthesis of CP-supported Pd/PdNi nanocatalysts was carried out according to the following steps. The CP was firstly immersed in a 0.1% (w/w) Triton X-100 solution for 24 h to reduce the paper hydrophobicity, according to [22]. The wet paper was then immersed in a large amount of pure water to remove the Triton X-100 and was dried in air for use. Meanwhile, $x \text{ mg}$ of PdCl_2 , $y \text{ mg}$ of $\text{NiCl}_2 \cdot 6\text{H}_2\text{O}$, and 3 mg of multiwalled carbon nanotube (CNT) were dissolved in 0.24 mL of water under sonication, and then, $60 \mu\text{L}$ of Nafion solution was added to form a uniform suspension. Next, $20 \mu\text{L}$ of the suspension was added dropwise onto the one side of the CP treated by Triton X-100. Addition of CNT particles leads to the well-dispersed metal salts when the suspension was dried and thus facilitates the reaction between NaBH_4 and the metal ions, as indicated in the next step. After drying in air, the CP was immersed in 10 mL of 5% (w/w) NaBH_4 solution and held on for 5 h. The CP was afterwards removed from the solution and put to a large amount of water until neutral water was obtained. At last, the CP was dried on a vacuum at $40 \text{ }^\circ\text{C}$ for 10 h to obtain the CP-supported Pd/PdNi nanocatalysts, which were marked by Pd-situ/CP at $x = 1 \text{ mg}$ and $y = 0 \text{ mg}$, Pd_9Ni_1 -situ/CP at $x = 1 \text{ mg}$ and $y = 0.15 \text{ mg}$, and Pd_8Ni_2 -situ/CP at $x = 1 \text{ mg}$ and $y = 0.34 \text{ mg}$. Figure 1 shows the schematic diagram of the preparation process of the samples. As indicated in Fig. 1, formation and deposition of the metal nanoparticles take place on the surface of the CNT and CP. For a comparison, a conventional CNT-supported Pd nanoparticles (Pd/CNT) with the Pd mass loading of 17% were firstly synthesized by NaBH_4 reduction reaction according to our recent report [21], and then, 5 mg of the Pd/CNT particles was added to 0.96 mL of ethanol

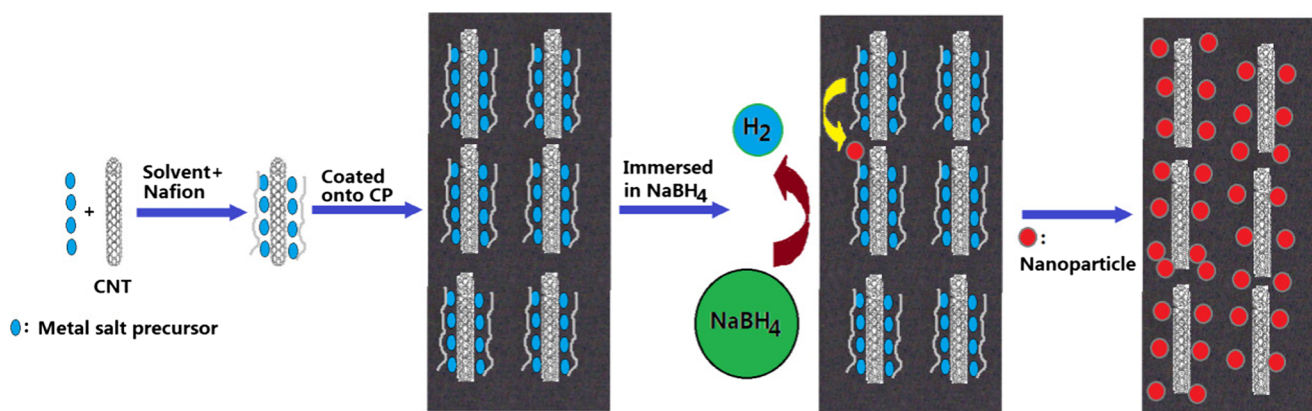


Fig. 1 Schematic diagram for in situ deposition of metal nanoparticles onto carbon paper

containing 40 μL of Nafion solution. After being subjected to sonication for 1 h, 50 μL of the as-obtained suspension was transferred onto the one side of the CP treated by Triton X-100, leading to the Pd/CNT particles dispersed on CP, named by Pd/CP. For the four prepared samples Pd-situ/CP, Pd₉Ni₁-situ/CP, Pd₈Ni₂-situ/CP, and Pd/CP, their Pd mass loading on CP was controlled to the same value (0.17 mg cm⁻²).

Crystalline phase compositions of the samples were studied with XRD obtained in a D/MAX2500X diffractometer (Japan), operating with Cu K alpha radiation generated at 40 kV and 250 mA ($\lambda = 0.15418$ nm). The surface structures of the samples were characterized by TEM images recorded in a JEM-2100F transmission electron microscopy.

Electrochemical measurements were carried out with an AutoLab PGSTAT30/FRA (Eco Chimie, The Netherlands) electrochemical workstation. A conventional three-electrode system was applied, where the Pd or PdNi nanocatalyst-modified glassy carbon (GC), Pt foil, and Ag/AgCl (in saturated KCl) were used as working, counter, and reference electrodes, respectively. All potentials reported in this paper were against the Ag/AgCl. For the EIS measurements, the amplitude of modulation potential was 10 mV, and the range of frequency was controlled from 40 kHz to 40 mHz. Geometrical area of the CP on which the catalyst particles were dispersed was controlled to be 0.25 cm² and was used to calculate the current density. All experiments were performed in room temperature.

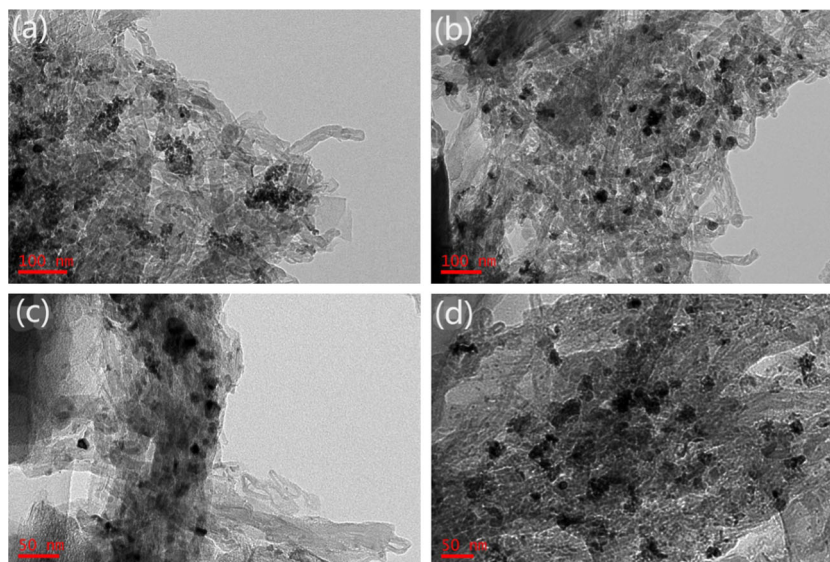
Results and discussion

Figure 2a shows large aggregates of Pd particles, which may be related to the preparation process of the Pd/CP [21]. Once the Pd²⁺ ions are reduced in solution, the as-formed Pd particles start to aggregate before they are deposited on CNT, leading to the

larger aggregates on CNT. This can be clearly seen from TEM image of the Pd/CP shown in Fig. 2a, where a number of large aggregates, composed of smaller particles with sizes of 4.5–7.1 nm, are formed. Thus, it is reasonable to infer that according to the fabrication of the Pd/CP, if the formation of Pd nanoparticles and their deposition on CNT take place on the same place (called “in situ synthesis”), the formation of the aggregates will be avoided or greatly reduced. TEM images of the Pd-situ/CP well support this hypothesis, as indicated in Fig. 2b. The Pd nanoparticles of the Pd-situ/CP sample are uniformly dispersed on CNTs, and no obvious aggregation between the Pd particles is observed. The sizes of the Pd nanoparticles of the Pd-situ/CP are 15–24 nm. As for the Pd₉Ni₁-situ/CP and Pd₈Ni₂-situ/CP samples (Fig. 2c, d), their particle sizes are 7–11 and 8–14 nm, respectively, and the catalyst particles exhibit relatively uniform distribution except for a small number of aggregates. This indicates that addition of Ni may decline the reduction of Pd ions, leading to the decrease of the size of Pd particles [35]. It is seen from the preparation process of the Pd-situ/CP, Pd₉Ni₁-situ/CP, and Pd₈Ni₂-situ/CP samples (Fig. 1) that reduction of metal precursors (metallic salts) is directly carried out on the surface of CNTs. The as-formed metal nanoparticles are therefore in situ immobilized on CNTs, reducing the chance for the particles to contact with each other. Figure 2c, d also shows that the boundary between the catalyst particles is relatively fuzzy, which may be caused by the presence of Ni oxides.

X-ray diffraction patterns of the Pd/CP, Pd-situ/CP, Pd₉Ni₁-situ/CP, and Pd₈Ni₂-situ/CP samples were recorded and are shown in Fig. 3. All samples exhibit a maximum peak located at 26.4° corresponding to the graphite (0 0 2) plane of CNT support. The weak diffraction peak at 54.5° is also ascribed to the (003) plane of CNTs. The diffraction peaks at 39.9°, 46.3°, 67.8°, and 81.5° are indexed to the (111), (200), (220), and (311) planes of Pd face-centered cubic (fcc) crystal structure.

Fig. 2 TEM images of the Pd/CP (a), Pd-situ/CP (b), Pd₉Ni₁-situ/CP (c), and Pd₈Ni₂-situ/CP (d) samples



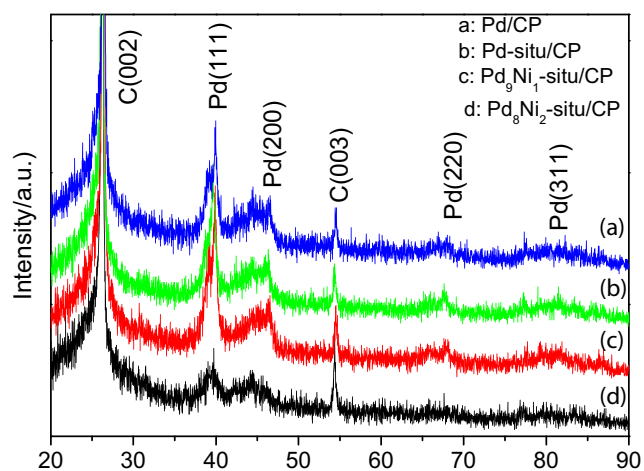


Fig. 3 X-ray diffraction patterns of the prepared samples

Note in Fig. 3 that there are no obvious fraction peaks involved in Ni due to the low contents of Ni in Pd₉Ni₁-situ/CP and Pd₈Ni₂-situ/CP samples. Indeed, XRD is mass sensitive, and if the reflection intensities of Ni are much lower than Pd, Ni will not be detected in the diffractograms. The Pd diffraction peaks of the binary PdNi catalysts maintain the same diffraction angle as the Pd/CP and Pd-situ/CP, showing that no alloy between Pd and Ni is formed in Pd₉Ni₁-situ/CP and Pd₈Ni₂-situ/CP catalysts. The Pd crystalline size of the as-synthesized samples can be estimated from the XRD data according to Scherrer's equation. And the (111) reflection of the Pd face-centered cubic (fcc) structure at 2θ of 39.9° is used to calculate the crystalline size from the following Scherrer's equation:

$$d(A^\circ) = \frac{0.89\lambda_{CuK}}{\beta_{2\theta}\cos\theta_{\max}} \quad (1)$$

where β is the width of half peak, λ is the incident wavelength, d is the particle diameter, and θ is the diffraction angle at peak maximum. The average crystalline size is thus reckoned to be

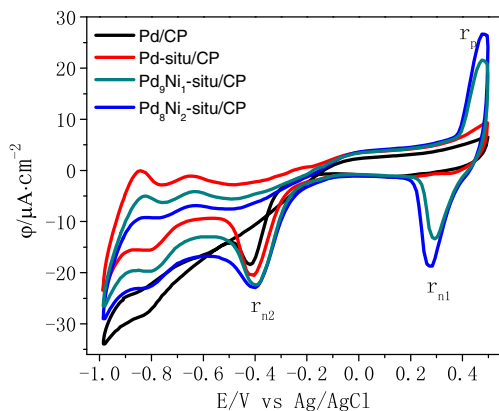


Fig. 4 Cyclic voltammograms of the samples in 1.0 mol L⁻¹ NaOH at a scan rate of 50 mV s⁻¹

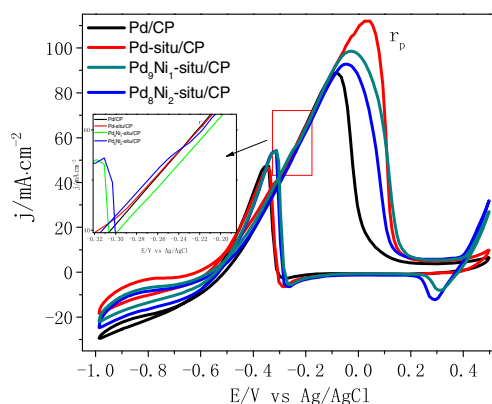


Fig. 5 Cyclic voltammograms of the samples in 1.0 mol L⁻¹ NaOH in the presence of 0.5 mol L⁻¹ ethanol at a scan rate of 50 mV s⁻¹. Inset is the zoomed main panel of the CVs

4.9 nm for Pd/CP, 5.8 nm for Pd-situ/CP, 5.1 nm for Pd₉Ni₁-situ/CP, and 5.2 nm for Pd₈Ni₂-situ/CP. These calculated data are less than those observed from TEM images, showing that the particles observed from TEM images are composed of a number of smaller crystal grains.

Cyclic voltammetric (CV) data on the prepared samples in 1 mol L⁻¹ NaOH solution were recorded as indicated in Fig. 4. It is observed from Fig. 4 that the samples show a characteristic reduction peak of polycrystalline Pd electrode at potentials of -0.39 to -0.42 V, which can be attributed to the reduction of Pd oxides produced during the forward potential scan. In contrast to the Pd/CP and Pd-situ/CP, Pd₉Ni₁-situ/CP and Pd₈Ni₂-situ/CP samples display a well-defined oxidation peak r_p at ca. 0.48 V and a reduction peak r_{n1} at 0.28~0.29 V, which are attributed to the formation and reduction of Ni(III) species, respectively. The real surface areas involved to Pd active sites (S_{activePd}) for the prepared samples can be reckoned according to the coulombs consumed for the reduction of Pd oxides (cathodic peak r_{n2}) formed during the forward scan on the smooth polycrystalline Pd electrode (CV not shown). S_{activePd} value of the Pd-situ/CP, Pd₉Ni₁-situ/CP, Pd₈Ni₂-situ/

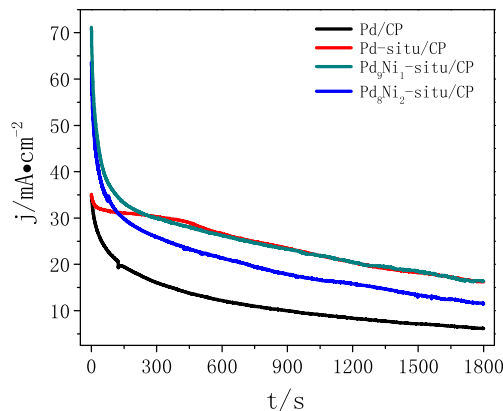
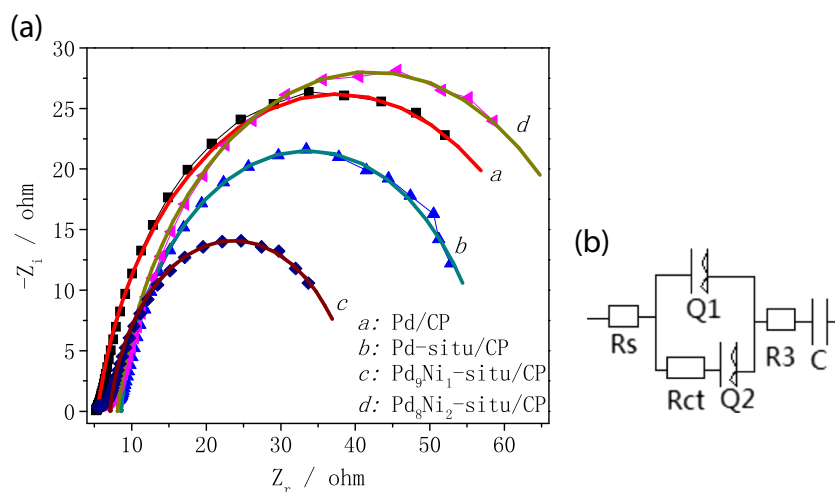


Fig. 6 Chronoamperometric responses of the samples in 1.0 mol L⁻¹ NaOH in the presence of 0.5 mol L⁻¹ ethanol at a potential of -0.25 V

Fig. 7 **a** Electrochemical impedance spectra of the samples in 1.0 mol L^{-1} NaOH in the presence of 0.5 mol L^{-1} ethanol at -0.25 V . Dots and corresponding lines present the experimental data and fitting values, respectively. **b** The equivalent electric circuit compatible with the Nyquist diagrams. *R_{ct}* charge transfer resistance, *R_s* electrolyte resistance, *Q* constant phase element (CPE), *C* capacitance, *R₃* resistance of the oxidation of the intermediates produced from alcohol oxidation

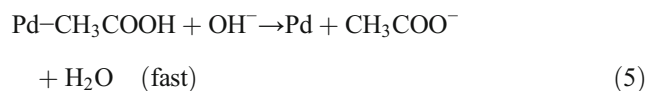
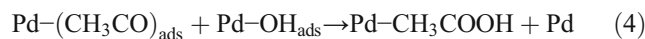
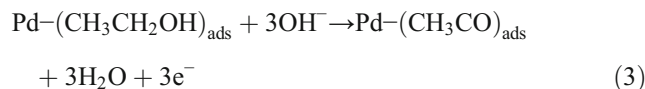
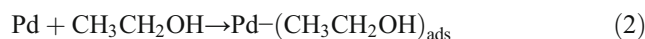


CP, and Pd/CP samples is 7.1, 7.8, 9.3, and 5.1 cm^2 , respectively, showing that the Pd and PdNi nanoparticles prepared by this in situ deposition method present larger active Pd surface area. This is consistent with the TEM images where highly dispersed metal nanoparticles of the Pd-situ/CP, Pd₉Ni₁-situ/CP, and Pd₈Ni₂-situ/CP samples were observed. It can be also seen that the addition of Ni enhances the synergistic effect of metals between Pd and Ni and thus improves the catalytic activity.

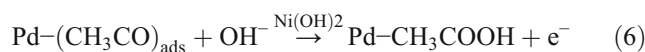
Figure 5 reveals CV data of the prepared samples in NaOH solution containing 0.5 mol L^{-1} ethanol. All samples present a typical anodic peak r_p for ethanol oxidation during the forward scan. The r_p peak current density on the Pd/CP, Pd-situ/CP, Pd₉Ni₁-situ/CP, and Pd₈Ni₂-situ/CP is 88.7, 112.7, 99.0, and 93.4 mA cm^{-2} , respectively. Also, the Pd-situ/CP, Pd₉Ni₁-situ/CP and Pd₈Ni₂-situ/CP exhibit a respective onset potential of -0.62 , -0.57 , and -0.55 V for ethanol oxidation, which present more negative shifts compared to that of -0.51 V on the Pd/CP. Results show that for Pd₉Ni₁-situ/CP and Pd₈Ni₂-situ/CP catalysts, the synergistic effect between Pd and Ni is not obvious due to the absence of the alloying of Pd and Ni, leading to their lower current densities and more positive onset potentials compared to the Pd-situ/CP catalyst. It is further found from Fig. 5 that the current density of ethanol oxidation displays a rapid rise from the onset potential to the peak r_p potential. In this potential range, the four samples also present different anodic current densities as indicated in the zoomed main panel, where the current density at the potential of -0.25 V on the Pd/CP, Pd-situ/CP, Pd₉Ni₁-situ/CP, and Pd₈Ni₂-situ/CP is 53.0, 53.4, 54.1, and 50.7 mA cm^{-2} , respectively. After the peak r_p , the anodic current density declines nearly to zero, which is caused by the formation of the Pd oxides at higher potentials. The peak r_p potentials on the Pd-situ/CP, Pd₉Ni₁-situ/CP, and Pd₈Ni₂-situ/CP, however, shift to more positive values, compared to that on the Pd/CP. This indicates that the formation of Pd oxides at higher anodic

potentials on these in situ synthesized Pd samples is suppressed. The rapid rise of the anodic current on the Pd₉Ni₁-situ/CP and Pd₈Ni₂-situ/CP commences at a potential of 0.4 V , caused by the formation of Ni(III) species. Subsequent cathodic peaks at $0.28\text{--}0.3 \text{ V}$ are related to the reduction of the Ni(III) species.

The mechanism of ethanol oxidation on Pd in alkaline media can be described according to the following reactions (2)–(5) [36]:



As for the binary Pd-Ni catalysts, Ni(OH)₂ and NiO are easily formed in alkaline media. In addition, ethanol oxidation is related to both (CH₃CO)_{ads} and OH_{ads}. Addition of Ni can increase the concentration of OH⁻ on the surface of catalyst, which could accelerate the ethanol oxidation to a certain extent. Therefore, the ethanol oxidation mechanism on Pd_xNi_y-situ/CP catalysts can be indicated by reactions (2), (3), and (6) [37]:



Chronoamperometric data of the prepared samples were recorded by maintaining the electrode at a constant potential of -0.25 V in a solution containing 0.5 mol L^{-1} ethanol and 1.0 mol L^{-1} NaOH, as indicated in Fig. 6. The Pd-situ/CP and Pd₉Ni₁-situ/CP present the highest current density compared to the Pd/CP and Pd₈Ni₂-situ/CP samples. It is clearly seen

from Fig. 6 that the maximum current density obtained is over 70 and 60 mA cm⁻² on Pd₉Ni₁-situ/CP and Pd₈Ni₂-situ/CP, respectively. Although almost the same maximum current density arises on Pd/CP and Pd-situ/CP, after that, the current density on the Pd-situ/CP is always significantly larger than that on the Pd/CP. Figure 6 also reveals that the Pd-situ/CP and Pd₉Ni₁-situ/CP exhibit a very close current density after holding the step time of 600 s, and the current densities from the samples synthesized by this “in situ method” are higher than

the current density measured for the Pd/CP sample. Moreover, the Pd-situ/CP or Pd₉Ni₁-situ/CP sample delivers a current density at 1800 s that is over 2.6 times larger than that for the Pd/CP sample. This reveals the highly stable current density of ethanol oxidation on the samples prepared by this in situ deposition.

Electrochemical reaction resistances of ethanol oxidation on the prepared samples were further studied through electrochemical impedance spectroscopic measurements. Figure 7 reveals the Nyquist plots of the samples at a potential of -0.25 V in 1 mol L⁻¹ NaOH containing 0.5 mol L⁻¹ ethanol. All samples exhibit a well-defined semicircle Nyquist plot in the range of the frequency studied, which is caused by the ethanol oxidation. The impedances on both the imaginary and real axes follow the order Pd₉Ni₁-situ/CP < Pd-situ/CP < Pd/CP < Pd₈Ni₂-situ/CP. The fitting curves shown in Fig. 7 are obtained from the equivalent electric circuit compatible with the corresponding Nyquist diagrams. It is clearly seen from the fitting curves that the equivalent circuit is well compatible with the electrochemical processes. The charge transfer resistance (R_{ct}) values for ethanol oxidation on Pd₉Ni₁-situ/CP, Pd-situ/CP, Pd/CP, and Pd₈Ni₂-situ/CP samples are 33.5, 49.6, 61.2, and 67.3 Ω, respectively. Results are consistent with the anodic current densities of ethanol oxidation at a potential of -0.25 on the prepared samples as indicated in CVs (Fig. 5).

Electrocatalytic stabilities of the as-synthesized samples for ethanol oxidation were investigated by cyclic voltammetry. Figure 8a–c shows 400 consecutive cyclic voltammograms of the Pd/CP, Pd-situ/CP, and Pd₉Ni₁-situ/CP samples in 1.0 mol L⁻¹ NaOH + 0.5 mol L⁻¹ ethanol at a scan rate of 50 mV s⁻¹. It is clearly seen from Fig. 8 that the anode current density on the forward-going scan declines with the increasing of the number of successive cycle sweep. According to the changes of the anode peak (*r_p*) current density on the forward-going scan, Pd₉Ni₁-situ/CP sample exhibits relatively higher electrocatalytic stability than Pd/CP and Pd-situ/CP. The *r_p*

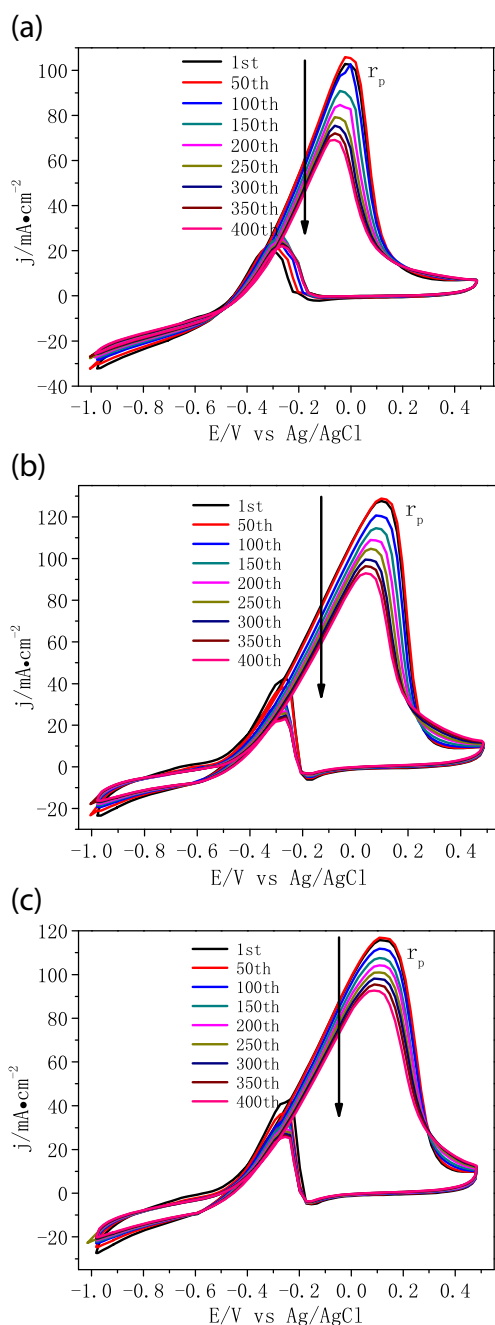


Fig. 8 Four hundred consecutive sweeps of cyclic voltammograms on the Pd/CP (a), Pd-situ/CP (b), and Pd₉Ni₁-situ/CP (c) in 1 mol L⁻¹ NaOH containing 0.5 mol L⁻¹ ethanol at a potential scan rate of 50 mV s⁻¹

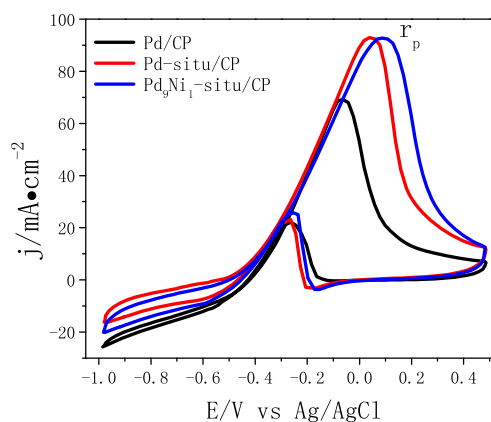
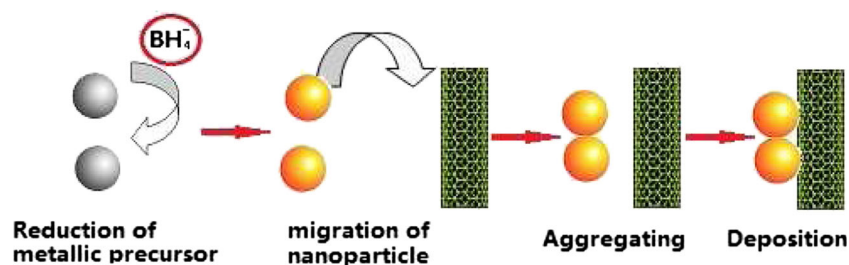


Fig. 9 The cyclic voltammograms at the 400th cycle obtained from Fig. 8. Others same as Fig. 8

Fig. 10 Schematic diagram for conventional synthesis of metallic nanoparticles



current densities for the 400th cycle on the Pd/CP, Pd-situ/CP, and Pd₉Ni₁-situ/CP samples are respectively 67, 73, and 80% of those for the first cycle. That means that the r_p peak current density on the Pd₉Ni₁-situ/CP sample keeps a slower falling with the cycle sweeping number, while those on the Pd/CP and Pd-situ/CP samples display a relatively rapid decline with the cycle sweeping number. Results show that an appropriate adding amount of Ni improves the stability of Pd catalyst.

Electrocatalytic stabilities of the prepared samples can be further seen from their CV profiles recorded at the 400th cycle. Figure 9 shows the CV curves at the 400th cycle on the Pd/CP, Pd-situ/CP, and Pd₉Ni₁-situ/CP catalysts in 1 mol L⁻¹ NaOH containing 0.5 mol L⁻¹ ethanol at a potential scan rate of 50 mV s⁻¹. It can be clearly seen from Fig. 9 that Pd-situ/CP and Pd₉Ni₁-situ/CP have higher r_p current densities than the Pd/CP. Results show that the samples prepared by the in situ deposition method possess higher electrocatalytic stability for ethanol oxidation.

The different electrocatalytic behaviors of Pd/CP and Pd-situ/CP samples can be attributed to their different deposition mechanisms. It is clearly seen from Fig. 1 that both production and deposition of metallic nanoparticles take place on the surface of CNTs. Immobilization of nanoparticles on CNTs reduces their surface energy and is beneficial to improve their stability, leading to the great reduction of the aggregation between the nanoparticles. By contrast, conventional synthesis of metallic nanoparticles undergoes such steps as reduction of metal precursor, migration of nanoparticles to a substrate, and immobilization on the substrate, as indicated in Fig. 10. The aggregation between the particles occurs during their migration to the surface of CNTs. The in situ deposition method proposed in this work is of therefore great significance for the synthesis of a substrate-supported catalyst with high electroactivity and electrostability.

Conclusions

In summary, we have proved the feasibility of in situ deposition of metal nanoparticles onto CP by immersing the CP, on which metal salts as the metal precursors have been loaded, into the NaBH₄ solution. Compared to the conventional synthesis of metal nanoparticles (Pd/CP), this new in situ

deposition method eliminates the filtration step and thus avoids the loss of catalyst particles. TEM images of the Pd and PdNi nanoparticles prepared by this new method (Pd-situ/CP and Pd-Ni-situ/CP) show that they are uniformly dispersed on CP without obvious aggregation between the particles. The as-fabricated Pd-situ/CP and Pd₉Ni₁-situ/CP samples reveal higher electrocatalytic activity and stability for ethanol oxidation than the Pd/CP. This study opens up an avenue to explore a new synthesis method of metal nanoparticles immobilized on a support for fuel cell applications.

Acknowledgements The financial support of this work by the National Natural Science Foundation of China (21376070) is gratefully acknowledged.

References

1. Barzegari MM, Dardel M, Alizadeh E, Ramiar A (2016) Dynamic modeling and validation studies of dead-end cascade H₂/O₂ PEM fuel cell stack with integrated humidifier and separator. *Appl Energy* 177:298–308
2. Monsalve K, Mazurenko I, Lalaoui N, Le Goff A, Holzinger M, Infossi P, Nitsche S et al (2015) A H₂/O₂ enzymatic fuel cell as a sustainable power for a wireless device. *Electrochem Commun* 60: 216–220
3. Thanganathan U (2016) Synthesis and characterization of hybrid composite membranes and their properties: single cell performances based on carbon black catalyst/proton-conducting hybrid composite membrane for H₂/O₂ fuel cells. *J Membr Sci* 517:100–110
4. Uma T, Mahalingam T, Kannan A, Cindrella L (2016) PEG based hybrid composite membranes and their properties for H₂/O₂ fuel cells. *Int J Hydrog Energy* 41:10896–10906
5. Neelakandan S, Kanagaraj P, Nagendran A, Rana D, Matsuura T, Muthumeenal A (2015) Enhancing proton conduction of sulfonated poly (phenylene ether ether sulfone) membrane by charged surface modifying macromolecules for H₂/O₂ fuel cells. *Renew Energy* 78: 306–313
6. Mikolajczuk-Zychora A, Borodzinski A, Kedzierzawski P, Mierzwa B, Mazurkiewicz-Pawlicka M, Stobinski L et al (2016) Highly active carbon supported Pd cathode catalysts for direct formic acid fuel cells. *Appl Surf Sci* 388:645–652
7. Wang K, Wang B, Chang J, Feng L, Xing W (2014) Formic acid electrooxidation catalyzed by Pd/SmOx-C hybrid catalyst in fuel cells. *Electrochim Acta* 150:329–336
8. Moreno-Zuria A, Dector A, Cuevas-Muñiz FM, Esquivel JP, Sabaté N, Ledesma-García J et al (2014) Direct formic acid microfluidic

- fuel cell design and performance evolution. *J Power Sources* 269: 783–788
9. Lesiak B, Mazurkiewicz M, Malolepszy A, Stobinski L, Mierzwa B, Mikolajczuk-Zychora A et al (2016) Effect of the Pd/MWCNTs anode catalysts preparation methods on their morphology and activity in a direct formic acid fuel cell. *Appl Surf Sci* 387:929–937
 10. Shen L, Li H, Lu L, Luo Y, Tang Y, Chen Y et al (2013) Improvement and mechanism of electrocatalytic performance of Pd–Ni/C anodic catalyst in direct formic acid fuel cell. *Electrochim Acta* 89:497–502
 11. Qi J, Benipal N, Liang C, Li W (2016) PdAg/CNT catalyzed alcohol oxidation reaction for high-performance anion exchange membrane direct alcohol fuel cell (alcohol = methanol, ethanol, ethylene glycol and glycerol). *Appl Catal B Environ* 199:494–503
 12. Figueiredo MC, Solla-Gullón J, Vidal-Iglesias FJ, Nisula M, Felio JM, Kallio T (2015) Carbon-supported shape-controlled Pt nanoparticle electrocatalysts for direct alcohol fuel cells. *Electrochem Commun* 55:47–50
 13. Carrión-Satorre S, Montiel M, Escudero-Cid R, Fierro JLG, Fatás E, Ocón P (2016) Performance of carbon-supported palladium and palladium single bond ruthenium catalysts for alkaline membrane direct ethanol fuel cells. *Int J Hydrog Energy* 41:8954–8962
 14. Figueiredo MC, Sorsa O, Doan N, Pohjalainen E, Hildebrand H, Schmuki P et al (2015) Direct alcohol fuel cells: increasing platinum performance by modification with sp-group metals. *J Power Sources* 275:341–350
 15. Jurzinsky T, Cremers C, Jung F, Pinkwart K, Tübke J (2015) Development of materials for anion-exchange membrane direct alcohol fuel cells. *Int J Hydrog Energy* 40:11569–11576
 16. Yi QF, Zou T, Zhang YY, Li XP, Xu GR, Nie HD et al (2016) A novel alcohol/iron (III) fuel cell. *J Power Sources* 321:219–225
 17. Yi QF, Chen QH (2015) In situ preparation and high electrocatalytic activity of binary Pd–Ni nanocatalysts with low Pd-loadings. *Electrochim Acta* 182:96–103
 18. Yi QF, Chu H, Tang MX, Yang Z, Chen QH, Liu XP (2015) Carbon nanotube-supported binary silver-based nanocatalysts for oxygen reduction reaction in alkaline media. *J Electroanal Chem* 739: 178–186
 19. Wang Y, Zhao Y, Yin J, Liu M, Dong Q, Su Y (2014) Synthesis and electrocatalytic alcohol oxidation performance of Pd–Co bimetallic nanoparticles supported on grapheme. *Int J Hydrog Energy* 39: 1325–1335
 20. Zhang M, Yan Z, Xie J (2012) Core/shell Ni@Pd nanoparticles supported on MWCNTs at improved electrocatalytic performance for alcohol oxidation in alkaline media. *Electrochim Acta* 77:237–243
 21. Yi QF, Chu H, Chen QH, Yang Z, Liu XP (2015) High performance Pd, PdNi, PdSn and PdSnNi nanocatalysts supported on carbon nanotubes for electrooxidation of C2–C4 alcohols. *Electroanalysis* 27:388–397
 22. Rego R, Oliveira C, Velázquez A, Cabot P-L (2010) A new route to prepare carbon paper-supported Pd catalyst for oxygen reduction reaction. *Electrochem Commun* 12:745–748
 23. Xu CW, Wang H, Shen PK, Jiang SP (2007) Highly ordered Pd nanowire arrays as effective electrocatalysts for ethanol oxidation in direct alcohol fuel cells. *Adv Mater* 19:4256–4259
 24. Xu CW, Cheng LQ, Shen PK, Liu YL (2007) Methanol and ethanol electrooxidation on Pt and Pd supported on carbon microspheres in alkaline media. *Electrochem Commun* 9:997–1001
 25. Zalineeva A, Serov A, Padilla M, Martinez U, Artyushkova K, Baranton S, Coutanceau C, Atanassov P (2015) Nano-structured Pd–Sn catalysts for alcohol electro-oxidation in alkaline medium. *Electrochem Commun* 57:48–51
 26. Modibedi RM, Masombuka T, Mathe MK (2011) Carbon supported Pd–Sn and Pd–Ru–Sn nanocatalysts for ethanol electro-oxidation in alkaline medium. *Int J Hydrog Energy* 36:4664–4672
 27. Jongsomjit S, Prapainainar P, Sombatmankhong K (2016) Synthesis and characterisation of Pd–Ni–Sn electrocatalyst for use in direct ethanol fuel cells. *Solid State Ionics* 288:147–153
 28. Yang GH, Zhou YZ, Pan HB, Zhu CZ, Fu SF, Wai CM, Du D, Zhu JJ, Lin YH (2016) Ultrasonic-assisted synthesis of Pd–Pt/carbon nanotubes nanocomposites for enhanced electro-oxidation of ethanol and methanol in alkaline medium. *Ultrason Sonochem* 28:192–198
 29. Luo WC, Zhou HH, Fu CP, Huang ZY, Gao N, Kuang YF (2016) Preparation and characterization of porous sponge-like Pd@Pt nanotubes with high catalytic activity for ethanol oxidation. *Mater Lett* 173:43–46
 30. Sieben JM, Alvarez AE, Comignani V, Duarte MME (2014) Methanol and ethanol oxidation on carbon supported nanostructured Cu core Pt–Pd shell electrocatalysts synthesized via redox displacement. *Int J Hydrog Energy* 39:11547–11556
 31. Hameed RMA (2017) Facile preparation of Pd–metal oxide/C electrocatalysts and their application in the electrocatalytic oxidation of ethanol. *Appl Surf Sci* 411:91–104
 32. Rostami H, Rostami AA, Omrani A (2016) An electrochemical method to prepare of Pd/Cu₂O/MWCNT nanostructure as an anode electrocatalyst for alkaline direct ethanol fuel cells. *Electrochim Acta* 194:431–440
 33. Song YY, Zhang XL, Yang S, Wei X, Sun ZB (2016) Electrocatalytic performance for methanol oxidation on nanoporous Pd/NiO composites prepared by one-step dealloying. *Fuel* 181:269–276
 34. Xu CW, Shen PK, Liu YL (2007) Ethanol electrooxidation on Pt/C and Pd/C catalysts promoted with oxide. *J Power Sources* 164:527–531
 35. He L, Gao JB, Yao ZL, Sun PY (2012) Characterization and catalytic performance evaluation of Pd/Ni/Al₂O₃ catalyst for hydrogenation of heavy reforming aromatic oil. *Pet Process Petrochem* 43: 39–43
 36. Liang ZX, Zhao TS, Xu JB, Zhu LD (2009) Mechanism study of the ethanol oxidation reaction on palladium in alkaline media. *Electrochim Acta* 54:2203–2208
 37. Zhang ZY, Xin L, Sun K, Li WZ (2011) Pd–Ni electrocatalysts for efficient ethanol oxidation reaction in alkaline electrolyte. *Int J Hydrog Energy* 36:12686–12697